The Institute of Space and Astronautical Science
Report No. 676, March 2000

Experimental Studies on Characteristics of Shock Wave Propagation through Cylinder Array

By

Kojiro SUZUKI*, Hiroaki HIMEKI**,
Tadaharu WATANUKI† and Takashi ABE††

(February 1, 2000)

ABSTRACT: The characteristics of the shock wave propagation through an array of cylinders perpendicular to the flow are experimentally investigated by using the shock tube. Quantitative and qualitative information on the attenuation of the transmitted shock wave, the pressure augmentation due to the reflected shock wave and the pressure oscillation in the wake due to shedding of the Kármán vortices is obtained from the unsteady pressure measurement. The schlieren pictures reveal the flow patterns of these features. Various cylinder arrangements are tested and their effects are discussed. The essential features of the propagation process are successfully simulated by the unsteady one-dimensional Euler analysis considering the drag force produced by the cylinder array. The drag force is evaluated by fitting the numerical results to the experimental data.

NOMENCLATURES

B	drag parameter of cylinder array (see eq. (3))
C_v	specific heat at constant volume
d	diameter of cylinder
E_t	total energy of flow per unit volume, $E_t=\rho\cdot(C_v\cdot T+u^2/2)$
f	peak frequency of pressure oscillation in the wake of cylinder array
F	drag coefficient of cylinder array (see eq. (5))
Ms	shock Mach number
p	pressure
$P1$	undisturbed pressure in test section (=atmospheric pressure) (see Fig. 10)
$P2$	pressure behind incident shock wave (see Fig. 10)
$P4$	initial pressure in the high pressure chamber of shock tube
$P5$	pressure behind transmitted shock wave (see Fig. 10)
$P6$	pressure behind contact surface (see Fig. 10)
$P7$	pressure behind reflected shock wave (see Fig. 10)

* Associate Professor, Graduate School of Frontier Sciences, The University of Tokyo
** Graduate Student, Graduate School of Engineering, The University of Tokyo
† Research Associate, Graduate School of Engineering, The University of Tokyo
†† Professor, The Institute of Space and Astronautical Science

Re_s	solid Reynolds number (see eq. (4))
St	Strouhal number of pressure oscillation in the wake of cylinder array (see eq. (1))
t	time
T	temperature
u	flow velocity
$U5$	flow velocity behind transmitted shock wave (see Fig. 10)
x	coordinate in shock tube axis

Greek symbols

β	drag force of cylinder array (see eq. (2))
ε	porosity (volume fraction of void) of cylinder array
μ	viscosity
ρ	density

1. INTRODUCTION

Considering the safety at an accidental explosion of the rocket, the launch site must be located far from the populated area. When the explosion occurs, a hemisphere-shaped shock wave is generated and propagates in the radial direction as shown in Fig. 1. The damage to the surrounding area is mainly caused by the rapid rise in the pressure due to the shock wave. In order to secure the safety in the populated area, the off-limits zone is set around the launch site, since the shock wave is weakened with the increase in the distance from the center of explosion. To determine the radius of the off-limits zone, which is often called as the "safety distance", the accurate prediction of the distance at which the shock wave is weakened to the safety level is necessary. However, the characteristics of the shock wave propagation are affected by the surface topography and the presence of obstacle around the launch site. In Japan, it is quite difficult to find a flat, clean and huge area for the launch site due to the limitation of the land. Hills and forest are commonly seen. As for the effects of the surface topography on the shock wave propagation, the precise computational studies have been made by Shimizu et al[1]. They clarified that the blast wave strength is significantly influenced by the ground surface geometry. However, the effects of the forest has not been clarified yet. To consider the characteristics of the shock wave propagation in the forest, we must know the drag force of the forest rather than the detailed flow pattern around each tree. In the present study, our interests are mainly focused on such overall features of the flow in an array of obstacles.

Lots of studies have been done on the shock wave propagation through a single obstacle both experimentally and computationally. For the shock wave through an array of obstacles, however, a little amount of studies have been made. Rogg et al[2]. experimentally investigated the shock-induced flow in an array of cylinders with staggered arrangement by using the shock tube. They compared the experimental results on the drag force of the cylinder array with the empirical relations. The detailed description of the unsteady flow field induced by the shock wave propagation in a cylinder array was obtained by Takayama et al[3,4], who used the interferograms to visualize both the experimental and computational flow field.

In the present study, the propagation of the shock wave through a cylinder array is experimentally investigated by using the shock tube. The flow in the forest is essentially three-dimensional and quite complicated. From a viewpoint of the overall features of the flow, however, the forest is regarded as a kind of porous media which produces the drag force to the incident flow. The shape of each obstacle is not important. Hence, we consider an array of cylinders to represent the forest in the experiment. In the case of an actual explosion, the shock wave propagation is three-dimensional. However, we

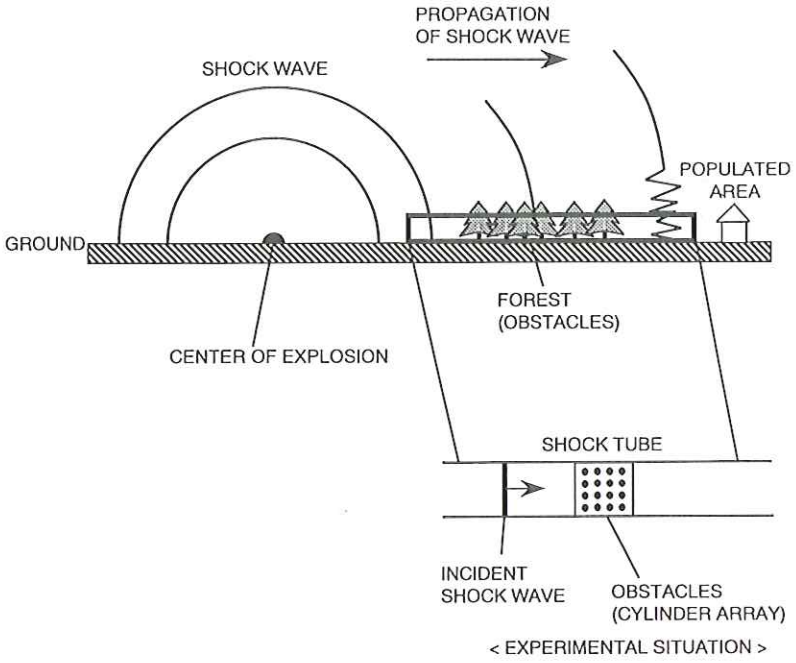

Fig. 1. Shock Wave Propagation at Accidental Explosion on the Ground and Situation of Present Experiment

consider the propagation of the normal shock wave in a channel having an array of cylinders as shown in Fig. 1, since such situation is easily obtained by using the shock tube. After these simplification of the problem, the essential properties of the phenomena are expected to be still retained. The propagation of the normal shock wave in the channel is described by the one-dimensional flow model. The drag force of a cylinder array is evaluated by considering the pressure difference between the upstream and downstream regions of the cylinder array. In the experiments, the unsteady pressure measurements are made at various locations in the channel. To consider the wide variety of the shape, diameter and the arrangement of trees in a forest, various cylinder arrangement and diameter are tested. The flow visualization by the schlieren method is made to reveal what happens at the interaction of the shock wave with a cylinder array.

The major objectives in the present study are as follows:

(1) To clarify the phenomena which occur at the propagation of the normal shock wave through a cylinder array with the emphasis on the attenuation and augmentation of the shock wave strength,

(2) To present a simple numerical model for description of such flow and evaluation of the drag force of a cylinder array,

(3) To investigate the effects of the cylinder arrangement and diameter.

2. EXPERIMENTAL METHODS AND APPARATUS

2. 1 Shock Tube

Figure 2 shows the schematic view of the experimental apparatus. The experiments are done by using the non-diaphragm type shock tube. It has the quick-action piston valve[5] in the high pressure chamber. In the present study, the high pressure chamber is charged up to 392-686 kPa (4-7 kgf/cm^2). When the piston valve is opened, the normal shock wave is generated in the circular duct and it goes into the square duct. The bore and length of the circular duct are 52.7 mm and 5700 mm, respectively.

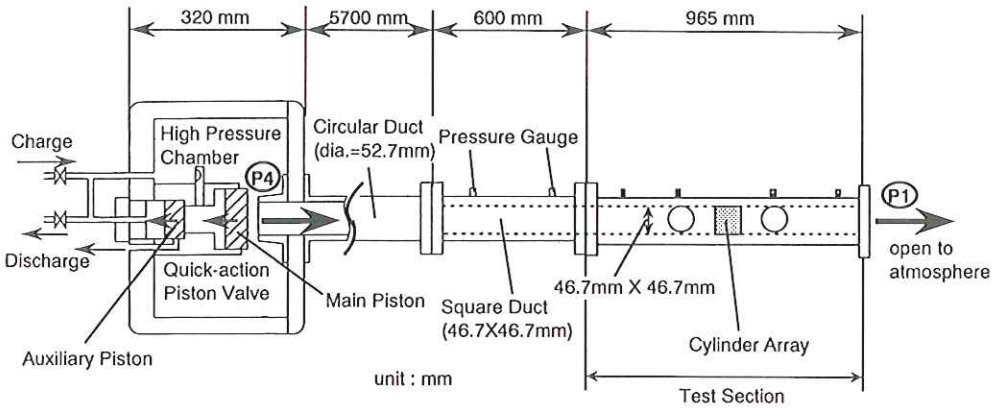

Fig. 2. Schematic View of Experimental Apparatus

In the square duct, the size of the cross section is 46.7 mm×46.7 mm. The area of the cross section is kept constant through the ducts. The test section, which has the same cross section shape as the square duct, is connected to the end of the square duct. The test section is open to the atmosphere. Hence, the initial pressure ratio of the shock tube ($P4/P1$) is varied from 4 to 7. At the interface between the circular duct and the square duct, the cross sectional shape is discontinuously changed from circle to square. The abrupt change in the cross section of the duct may cause the disturbances on the shock wave surface. In order to damp such disturbance before the shock wave reaches the test section, the length of the square duct should be long enough. In the present case, the length-to-height ratio of the square duct is set as about 12.8.

2. 2 Test Section

The configuration of the test section is shown in Fig. 3. The test section is the channel with 46.7 mm square cross section. The length is 965 mm. It has the cylinder array mount, eight static pressure ports and ten schlieren windows. The pressure ports are numbered #1, #2, ... , #8 from the upstream as shown in the figure. The pressure ports #1, 2, 6 and 8 are located on the ceiling of the test section. The others are on the side wall. Cylinders are set with their axes normal to the side wall. The high

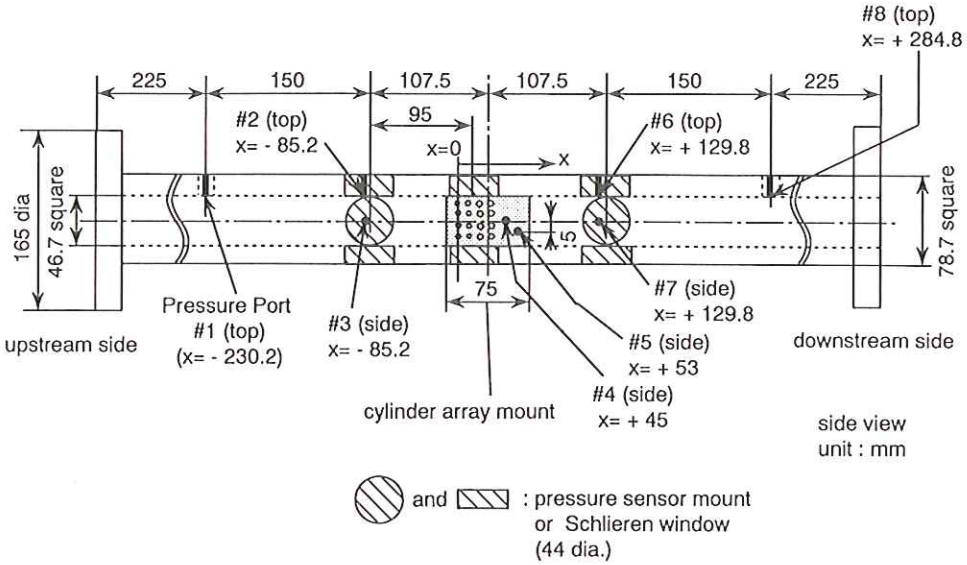

Fig. 3. Configuration of Test Section

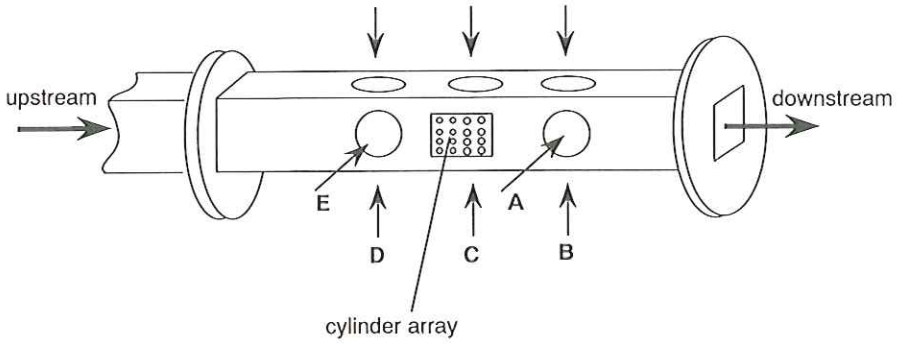

Fig. 4. Viewing Windows for Schlieren Picture

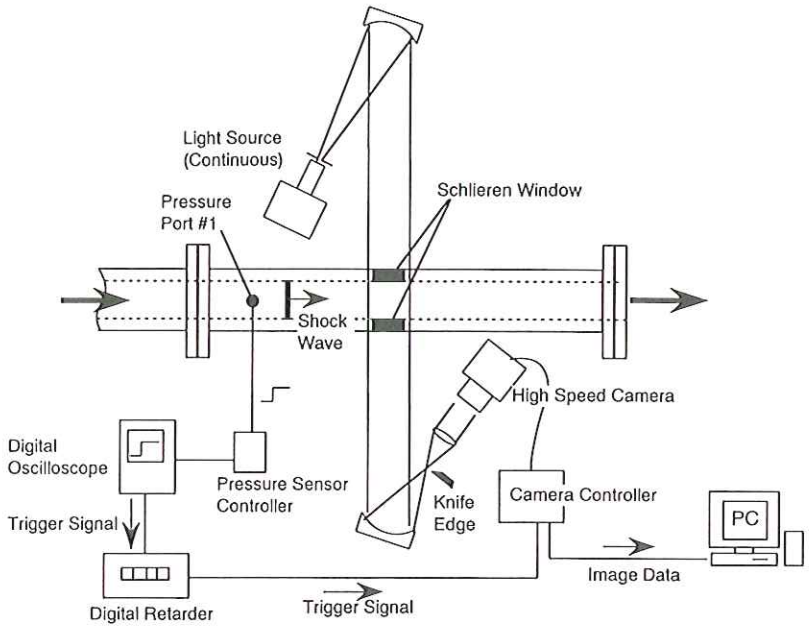

Fig. 5. Flow Visualization System

frequency quartz pressure transducer (PCB® Piezotronics Model 113A26) is mounted flush on each pressure port. The signal of the pressure transducer is recorded by the digital oscilloscope. Due to the limitation of the channels available on the oscilloscope, four ports are selected for the pressure measurement at a single shot of the shock tube.

Figure 4 shows the viewing directions of the schlieren picture. In the test section, five viewing directions (A-E) are available. The shock-induced flow field in the upstream, center, downstream of the cylinder array is visualized using these windows. The flow visualization system is shown in Fig. 5. When the pressure rise due to the incident shock wave is detected at port # 1, the trigger signal is sent to the camera controller after some delay time which is controlled by the digital retarder. The image is recorded by the high speed CCD camera with the image intensifier (NAC DiCAM-2). The shutter speed is set as 1 μsec. In such short duration, the shock wave seems almost stationary.

2. 3 Cylinder Array

Cylinders are set in the test section with their axes normal to the flow direction. We use two types of cylinder array mounts, that is, the regular arrangement and the staggered arrangement. Figure 6

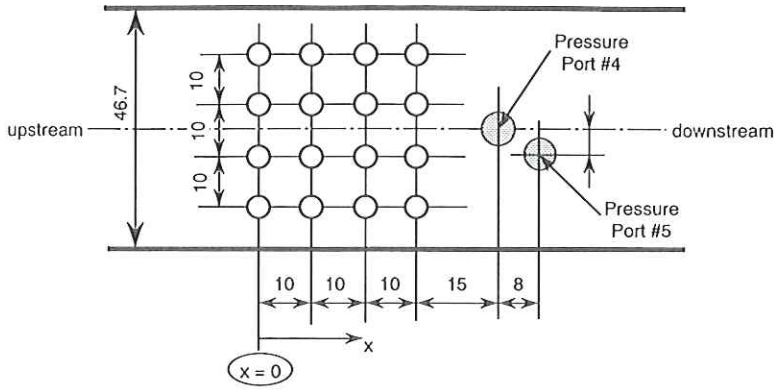

< Regular Arrangement >

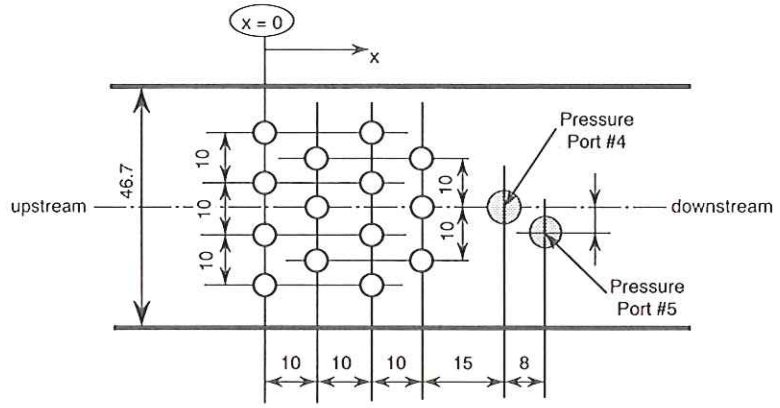

< Staggered Arrangement > unit : mm

Diameter of Cylinder = 4 mm, 8 mm
Diameter of Pressure Sensor Element = 5.5 mm

Fig. 6. Regular and Staggered Cylinder Arrangements

shows the positions of the cylinders for both arrangements. By selecting the type of array mount and the connectors to set cylinders, various patterns of the cylinder arrangement are available. For connectors not in use, small plugs are inserted to make the wall of the test section flat and smooth. The nominal cylinder diameter is 4 mm. The large cylinders with 8 mm diameter are also tested to investigate the effects of the cylinder diameter. Note that the diameter of the pressure sensor element is 5.5 mm and it is too large to resolve the spatial variation of the pressure in the scale smaller than the cylinder diameter.

The cylinder arrangements tested in the present experiment are divided into seven categories as listed in Table 1. In the table, the illustration of the cylinder arrangement is also given. For convenience of discussion, each cylinder arrangement is identified by the code number consisting of four digit number and alphabets. The first digit represents the number of cylinders in the most upstream row. The second, third and fourth digit numbers are defined in the same way. Note that we call the line of cylinders in the incident flow direction and that in the transverse direction as "column" and "row", respectively. The alphabet "R", "S" and "L" denote the regular arrangement, staggered arrangement (see Fig. 6) and the large cylinders, respectively.

The effects of the number of cylinders in the single row arrangement and in the single column arrangement are investigated in the categories I and II, respectively. In the category III, four cylinders are set in a row and the effects of the number of rows are studied. The case of 4444-R is the most packed arrangement in the present experiments. By comparing the results of the category II with those of the category IV, and comparing the category III with V, the effects of the staggered arrangement will be clarified. The effects of randomness in the cylinder arrangement and the effects of the cylinder diameter are investigated in the category VI and VII, respectively.

3. RESULTS AND DISCUSSIONS

3.1 Incident Shock Wave

Prior to discussing the experimental results for cylinder arrays, we describe the basic characteristics of the shock tube that is presently used. Figure 7 shows the typical pressure records at port #1, 4, and 8. There are no cylinders in the test section. The initial pressure in the high pressure chamber ($P4$) is set as 490 kPa (5 kgf/cm^2). At each port, almost the same level of pressure rise due to the incident shock wave is observed. The overshoot in the pressure rise at port #8 is expected to be caused by the slightly recessed (less than 0.5 mm) mount of the pressure gauge in order to protect the sensor from the impact of dusts in the test section. The shock velocity is calculated from the time lag of the pressure rise. The results show that the shock wave propagates at almost constant speed through the test section.

At port #8 in Fig. 7, the pressure gradually decreases after the plateau behind the shock wave. Such decrease is caused by the expansion wave from the exit of the test section, since the test section is open to the atmosphere and the expansion wave is produced at its end when the shock wave reaches there. The expansion wave propagates upstream in the test section and the time of its arrival determines the effective test duration. The arrival of the contact surface at the test section is much later than that of the reflected expansion wave. In the present experiments, the effective test duration is about 2 msec from the time when the shock wave arrives at port #1.

Figure 8 shows the variation of the shock Mach number with the initial pressure ratio ($P4/P1$).

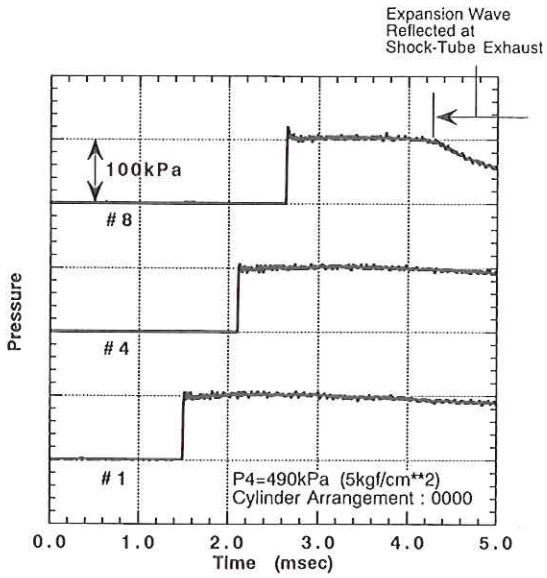

Fig. 7. Pressure Records in the Case of No Cylinders in Test Section

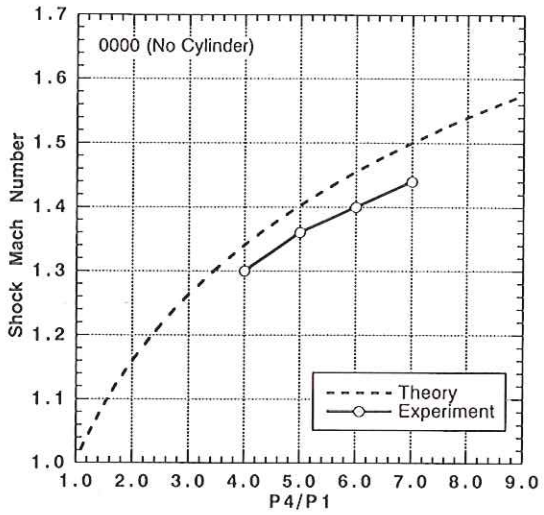

Fig. 8. Variation of Shock Mach Number with Initial Pressure Ratio of Shock Tube

The experimental shock Mach number is slightly smaller than the one-dimensional inviscid theory[6] because of the time required for valve opening and the three-dimensional effect of the flow around the piston valve.

The schlieren picture shows that a plain and undisturbed normal shock wave is generated in the test section. Disturbances due to the change in the cross section shape at the junction between the circular duct and the square duct are not observed. The repeatability of the experimental results is quite good both in the pressure measurement and in the flow visualization.

3. 2 Interaction of Shock Wave with Cylinder Array

Figure 9 shows the typical pattern of the pressure records in the far upstream (port # 1), just after the cylinders (#4) and in the far downstream (#8). The cylinder arrangement is 4444-R (see Table 1). The results in the absence of cylinders are also shown for comparison. The effects of the presence of the cylinder array are summarized by the features:

(1) pressure augmentation in the upstream region due to the shock wave reflected at the cylinder array,

(2) significant pressure oscillation just after the cylinder array,

(3) pressure attenuation in the transmitted shock wave and slight slowdown of its velocity.

The wave diagram of the present flow is schematically shown in Fig. 10. For convenience of discussion, each state is numbered as indicated in the figure.

Pressure Augmentation in the Upstream Region due to Reflected Shock Wave

The incident shock wave is partially reflected at the cylinder array. The reflected shock wave propagates upstream and the pressure augmentation occurs as seen in port # 1 of Fig. 9. The pressure rise due to the reflected shock wave seems slightly diffusive and the plateau portion after it becomes oscillatory in comparison with the incident shock wave, since the reflection does not occur instantaneously in the cylinder array. The schlieren picture in the upstream region of the cylinder array (Fig. 11) shows that the reflection does not occur as a single wave and that it consists of a couple of shock waves.

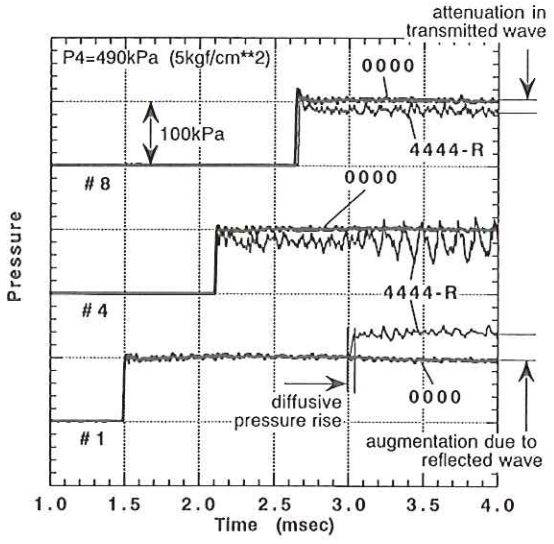

Fig. 9. Pressure Records for Cylinder Arrangement 4444-R

Table 1. Cylinder Arrangement for Present Experiments (1)

CATEGORY	NO. OF CYLINDERS	CYLINDER DIAMETER	CODE	CYLINDER ARRANGEMENT (○=OFF, ●=ON)
–	0	4 mm	0000	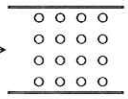
I Single Row	1	4 mm	0001-S	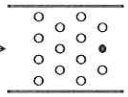
	2		0002-R	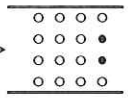
	3		0003-S	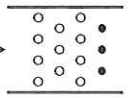
	4		0004-R	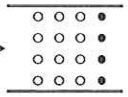

Table 1. Cylinder Arrangement for Present Experiments (2)

CATEGORY	NO. OF CYLINDERS	CYLINDER DIAMETER	CODE	CYLINDER ARRANGEMENT (○=OFF, ●=ON)
II Single Column	1	4 mm	0001-R	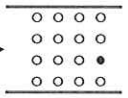
	2		0011-R	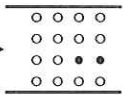
	3		0111-R	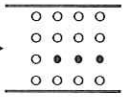
	4		1111-R	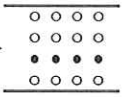
	2		0101-R	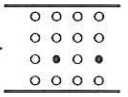
	2		1001-R	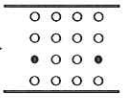

Table 1. Cylinder Arrangement for Present Experiments (3)

CATEGORY	NO. OF CYLINDERS	CYLINDER DIAMETER	CODE	CYLINDER ARRANGEMENT (○=OFF, ●=ON)
III Regular Multi-Rows	4	4 mm	0004-R	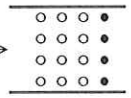
	8		0044-R	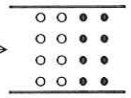
	12		0444-R	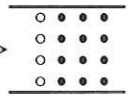
	16		4444-R	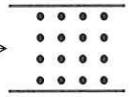
	8		0404-R	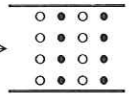
	8		4004-R	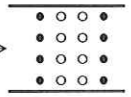

Table 1. Cylinder Arrangement for Present Experiments (4)

CATEGORY	NO. OF CYLINDERS	CYLINDER DIAMETER	CODE	CYLINDER ARRANGEMENT (○=OFF, ●=ON)
IV Staggered, Two Columns	2	4 mm	0011-S1	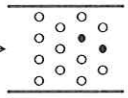
	3		0111-S1	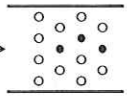
	4		1111-S1	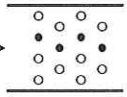
	2		0011-S2	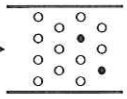
	3		0111-S2	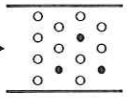
	4		1111-S2	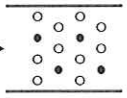

Table 1. Cylinder Arrangement for Present Experiments (5)

CATEGORY	NO. OF CYLINDERS	CYLINDER DIAMETER	CODE	CYLINDER ARRANGEMENT (○=OFF, ●=ON)
V Staggered, Multi-Rows	7	4 mm	0043-S	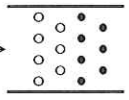
	14		4343-S	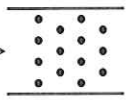
VI Staggered, Random	8	4 mm	4121-S1	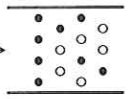
	8		4121-S2	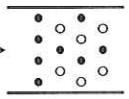
	8		4112-S1	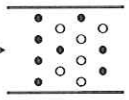
	8		4112-S2	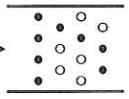

Table 1. Cylinder Arrangement for Present Experiments (6)

CATEGORY	NO. OF CYLINDERS	CYLINDER DIAMETER	CODE	CYLINDER ARRANGEMENT (○=OFF, ●=ON)
VII Large Cylinders	1	8 mm	0001-S-L	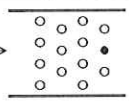
	2		0002-S-L	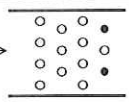
	2		0101-S-L	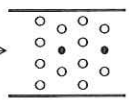
	2		0101-R-L	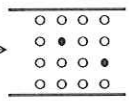
	2		0101-S-L	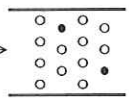

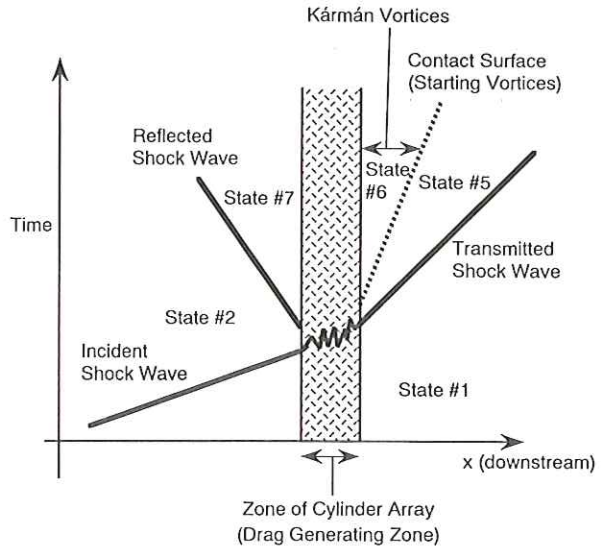

Fig. 10. Wave Diagram in the Presence of Cylinder Array

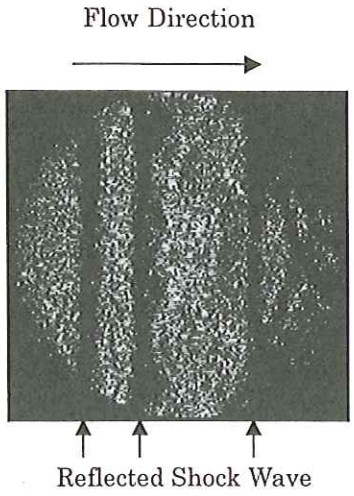

View from Window D
Cylinder Arrangement : 4444-R
0.89 msec after arrival of incident shock at port #1

Fig. 11. Schlieren Picture of Reflected Shock Wave

Pressure Oscillation in the Wake of Cylinders

In the present experiments, the flow behind the incident shock wave is subsonic and the wake behind the cylinders is expected to be similar to that in the incompressible flows. When the flow passes through the cylinder array, the starting vortices are generated and convected downstream. The starting vortices are expected to be located at the contact surface indicated in the wave diagram (Fig. 10), since they are convected at the flow velocity behind the transmitted shock wave, which is denoted by $U5$. Figure 12 shows the schlieren pictures of the starting vortices for the cylinder arrangement 0002-R. Comparison of the view in the direction of the cylinder axis (window A) and the spanwise view (window B) indicates that the wake flow behind the cylinders is almost two-dimensional. The

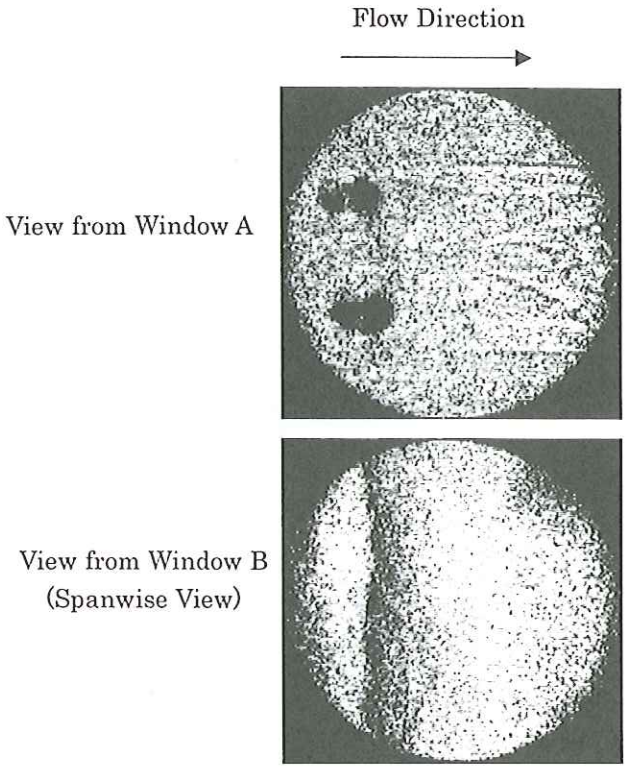

Cylinder Arrangement : 0002-R
1.26 msec after arrival of shock wave at port #1

Fig. 12. Schlieren Pictures of Starting Vortices

Kármán vortex street follows the starting vortices in state #6 of the wave diagram (Fig. 10). The view from window C (the spanwise view of the cylinders and their near wake) is shown in Fig. 13. The lines in parallel to the cylinder axis indicate the formation of the Kármán vortices. The propagation of the reflected shock wave is also seen in this figure. The Kármán vortices cause the cyclic oscillation of the pressure in the wake region of the cylinder array as observed in port #4 of Fig. 9. In this case, the Strouhal number of the pressure oscillation and the Reynolds number referred to the cylinder diameter and the local flow velocity ($U5$) is 0.24 and 5×10^4, respectively. The Strouhal number of 0.24 is close to 0.2 which is known as that for a cylinder in the freestream of the same Reynolds number range.

Pressure Attenuation in Transmitted Shock Wave

When the incident shock wave passes through the cylinder array, it is attenuated due to the drag force of the cylinders as seen in port #8 of Fig. 9. The arrival of the transmitted shock wave is slightly delayed in comparison with the case in the absence of cylinders. The pressure oscillation is not so significant as that in port #4, since the convection of the vortices is slower than the propagation of the transmitted shock wave and the starting vortices have not arrived at port #8 by the end of the test duration (see Fig. 10). It should be noted that the pressure attenuation in the transmitted shock wave in the downstream region of the cylinder array is smaller than the pressure augmentation due to the reflected shock wave in the upstream region.

Figure 14 shows the schlieren pictures of the transmitted shock wave. The diamond-shaped cell pattern is observed behind the shock front. When the number of cylinders increases, the cell size becomes smaller and the number of cells increases. Such pattern is expected to be caused by the

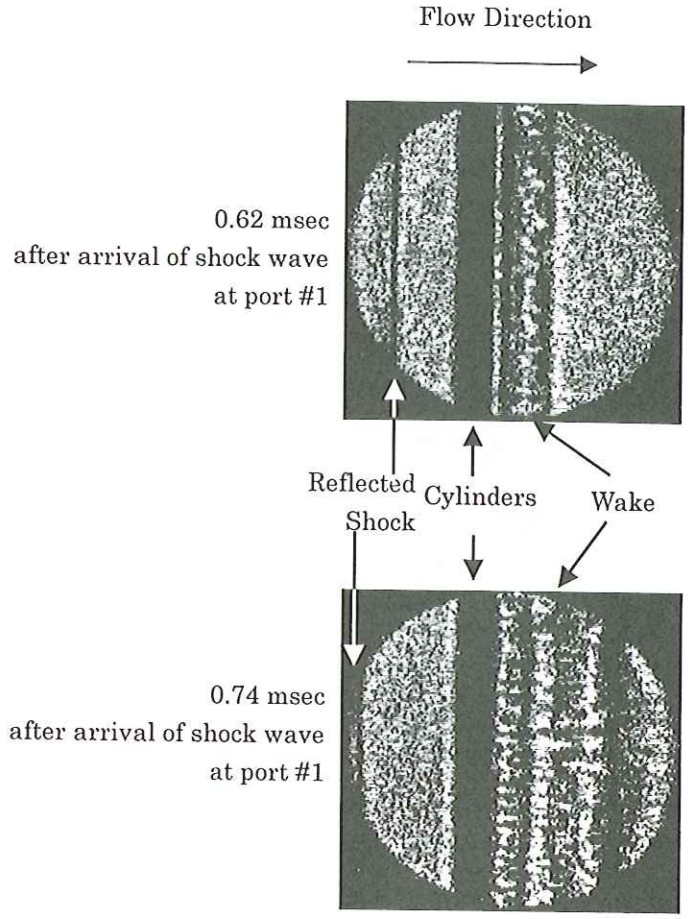

Cylinder Arrangement : 0200-R
View from Window C (Spanwise View)

Fig. 13. Schlieren Pictures of Kármán Vortex Shedding

diffraction of the incident shock wave at the cylinders and the reflection of these diffraction waves at the test section wall. To reveal the precise mechanism of formation of such pattern, the viewing area of the schlieren picture should be much wider to cover both the near and far downstream regions.

Three-dimensional Effects in Flow Field

In the present experiments, the three-dimensional effects on the flow are expected to be quite small. Figure 15 shows the schlieren pictures of the transmitted shock wave from window A (view in the direction of cylinder axis) and window B (spanwise view). The cylinder arrangement is 4444-R. The complicated diamond-shaped cell pattern is observed only from window A. This means that the flow is almost uniform in the spanwise direction. The similar observation is obtained in Figs. 12 and 13.

The pressure records at ports #2, 3 and ports #6, 7 show that the pressure depends mainly on the streamwise location and that there is no significant pressure gradient on the transverse plane normal to the shock tube axis. Consequently, the one-dimensional model is appropriate to describe the flow in the present experiments.

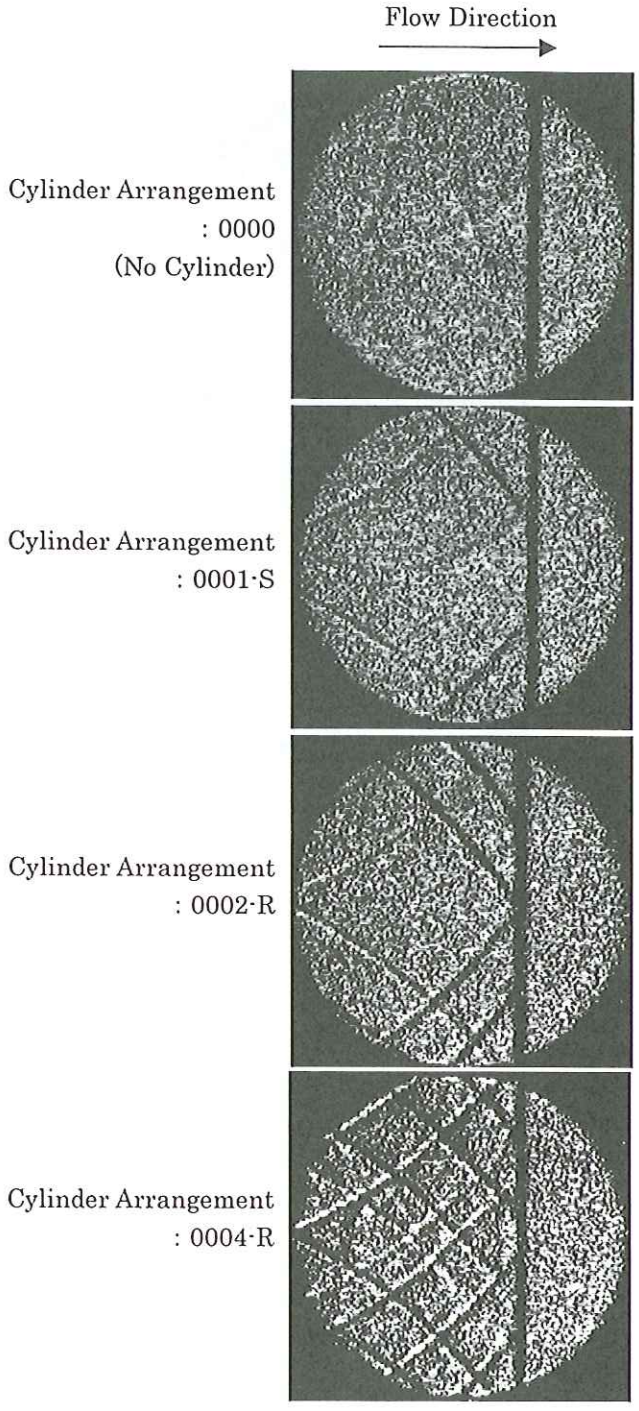

Fig. 14. Schlieren Pictures of Transmitted Shock Wave for Various Cylinder Arrangement

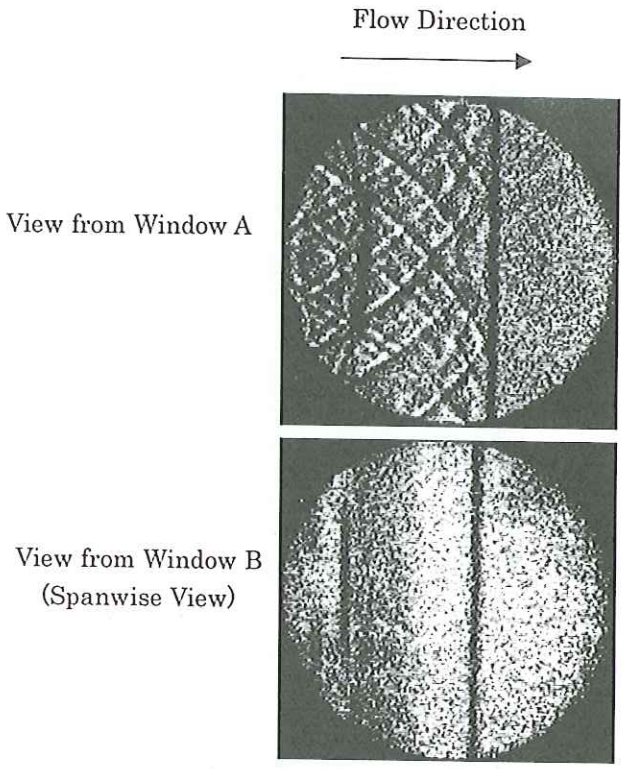

Fig. 15. Schlieren Pictures of Transmitted Shock Wave in Different Viewing Directions

3. 3 Effects of Cylinder Arrangement

We evaluate the overall features of the interaction of the shock wave with the cylinder array by the pressure of the transmitted shock wave (denoted by $P5$), the pressure behind the reflected shock wave ($P7$), and the Strouhal number (St) of the pressure oscillation in the wake ($P6$). By testing various cases listed in Table 1, the effects of the cylinder arrangement on these values are clarified as follows:

Attenuation of Transmitted Shock Wave in Single Row or Single Column Arrangement

Figure 16 shows the effect of the number of cylinders on the pressure behind the transmitted shock wave ($P5$) for the single row arrangement and single column arrangement (for definition, see the category I and II in Table 1). The initial pressure ratio ($P4/P1$) of the shock tube is varied from 4.0 to 7.0. In the case of the single row arrangement, the pressure behind the transmitted shock wave decreases with the increase in the number of cylinders. In the case of the single column arrangement, however, $P5$ is hardly affected by the number of cylinders. In the case of the single column arrangement, the effect of the distance between cylinders is investigated but it is negligibly small. Consequently, the attenuation of the transmitted shock wave mainly depends on the maximum blockage ratio of the cylinders in the channel.

Attenuation of Transmitted Shock Wave in the Case of Four Cylinders in a Row

In the case that there are four cylinders in a row (category III in Table 1), the pressure behind the

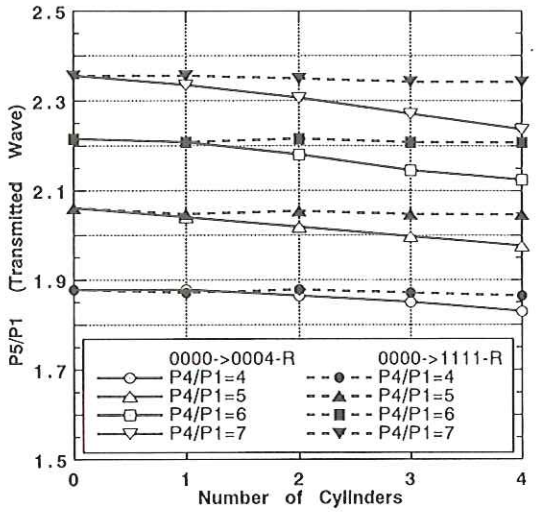

Fig. 16. Variation of Pressure behind Transmitted Shock Wave with the Number of Cylinders for Single Row and Single Column Arrangements

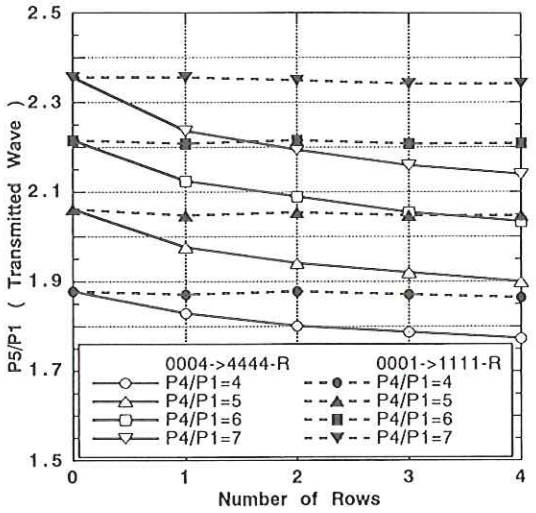

Fig. 17. Variation of Pressure behind Transmitted Shock Wave with the Number of Rows for the Cases of One Cylinder in a Row and Four Cylinders in a Row

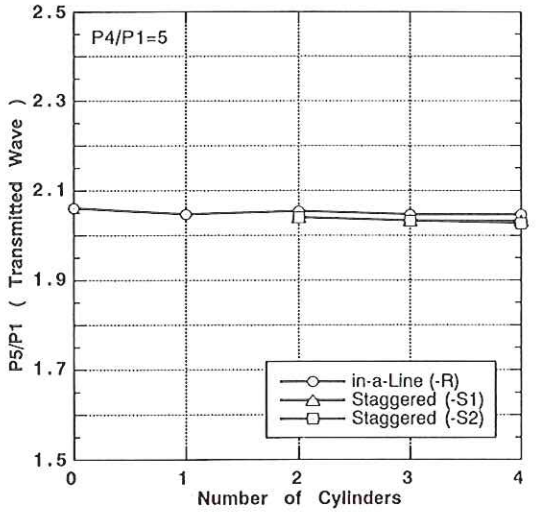

Fig. 18. Effects of Staggered Arrangement of Cylinders on Pressure behind Transmitted Shock Wave for Single Column Arrangement

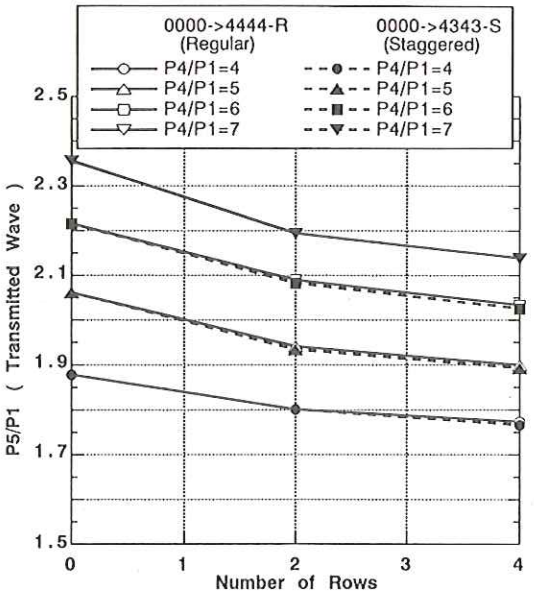

Fig. 19. Effects of Staggered Arrangement of Cylinders on Pressure behind Transmitted Shock Wave for Packed Cylinder Arrangement

transmitted shock wave decreases with the increase in the number of rows as shown by the solid lines in Fig. 17. In the case that there is only one cylinder in a row, the effect of the number of rows is negligibly small as shown by the dashed lines in the figure. When the cylinders are packed in a row, the drag force of the cylinder array depends on the length of the array in the flow direction. The effect of the distance between two rows is negligibly small.

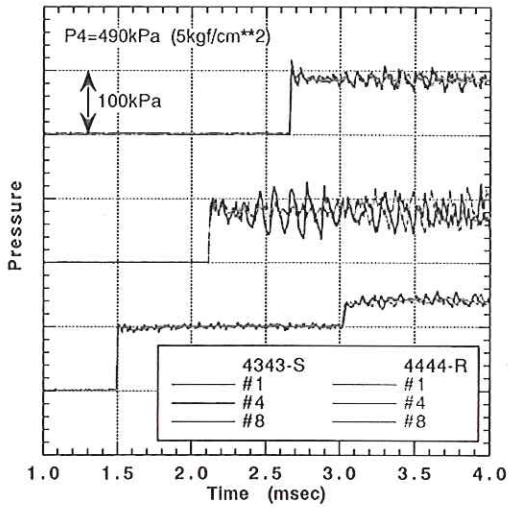

Fig. 20. Effects of Staggered Cylinder Arrangement on Pressure Records

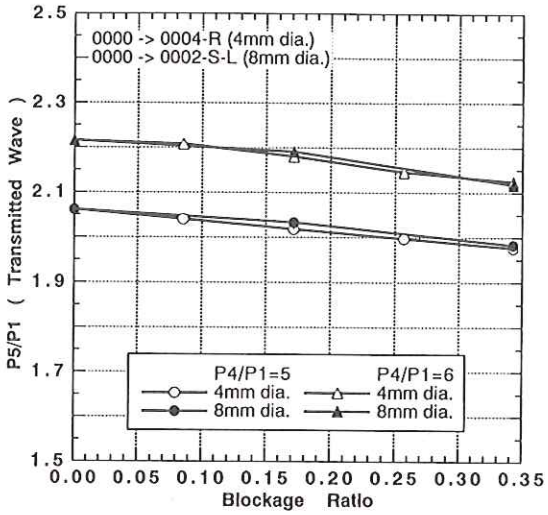

Fig. 21. Variation of Pressure behind Transmitted Shock Wave with Blockage Ratio

Effects of Staggered Arrangement on Transmitted Shock Wave

Figure 18 shows the comparison between the regular arrangement and the staggered arrangement with respect to the pressure behind the transmitted shock wave in the case of one cylinder in a row (category IV in Table 1). The comparison in the case of multi-cylinders in a row (categories III and V) is presented in Fig. 19. In both cases, the difference between the regular (in-a-line) arrangement and the staggered arrangement is quite small. In the pressure record at port #4 (near wake region), however, the oscillation seems more significant for the staggered arrangement than for the regular arrangement as shown in Fig. 20.

Effects of Cylinder Diameter on Transmitted Shock Wave

Figure 21 shows the variation of the pressure behind the transmitted shock wave with the blockage ratio for the single row arrangement. Note that the blockage ratio for one cylinder of 8 mm diameter is the same as that for two cylinders of 4 mm diameter. The curve for the 4 mm diameter cylinder almost coincides with that for the 8 mm diameter cylinder. The attenuation of the transmitted shock wave depends not on the cylinder diameter but on the blockage ratio.

Augmentation in Reflected Shock Wave and Attenuation in Transmitted Shock Wave

Figure 22 shows the variations of the pressure behind the transmitted wave ($P5$) and the pressure behind the reflected wave ($P7$) with the number of cylinders in the cases of the regular arrangement (category III), staggered arrangement (category V) and random arrangement (category VI) in Table 1. The pressure augmentation due to the reflected shock wave in the upstream region of the cylinder array is much larger than the pressure attenuation of the transmitted shock wave. Both the pressure attenuation in the downstream and the pressure augmentation in the upstream seem to depend mainly on the number of cylinders, in other words, porosity (volume fraction of void).

Strouhal Number of Pressure Oscillation in Wake Region

Figure 23 shows the power spectrum of the pressure oscillation at port #4 located in the near wake of the cylinder array. The cylinder arrangement is 0004-R and the initial pressure ratio of the shock tube is 5.0. A distinct peak is observed around 10 kHz. This peak is expected to represent the frequency of the Kármán vortex shedding. The variation of the Strouhal number with the number of

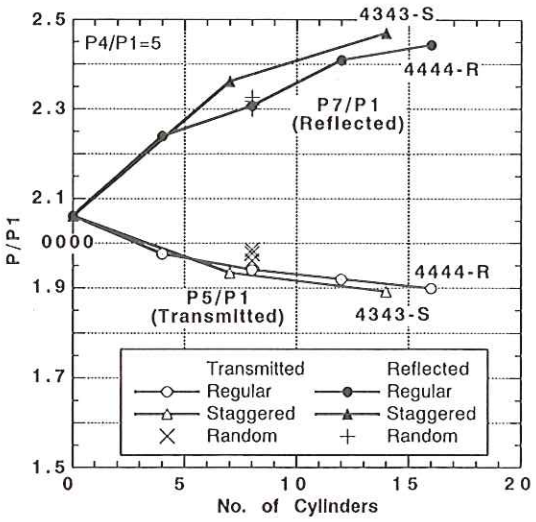

Fig. 22. Variations of Pressure behind Transmitted and Reflected Shock Waves with the Total Number of Cylinders

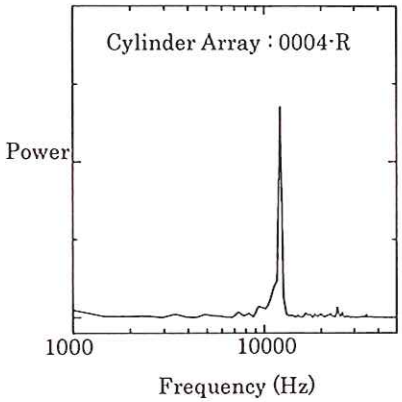

Fig. 23. Power Spectrum of Pressure Oscillation in Wake of Cylinder Array

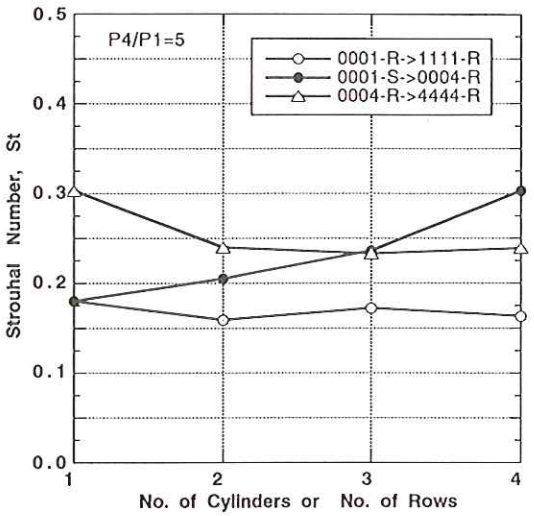

Fig. 24. Strouhal Number of Pressure Oscillation in Wake of Cylinder Array

cylinders or the number of rows is shown in Fig. 24. The Strouhal number St is defined by:

$$St = \frac{f \cdot d}{U5}, \qquad \cdots\cdots (1)$$

where f, d and $U5$ are the peak frequency, cylinder diameter and flow velocity behind the transmitted shock wave, respectively. The value of $U5$ is calculated from the velocity of the transmitted shock wave by using the Rankine-Hugoniot relations. In the case of the single column arrangement (0001-R, 0011-R, 0111-R and 1111-R), the Strouhal number is hardly affected by the number of the cylinders. In the case of the single row arrangement (0001-R, 0002-R, 0003-R and 0004-R), the Strouhal number increases with the increase in the number of cylinders, since the flow through the cylinders is accelerated by increasing the blockage ratio and the rise in the local flow velocity results in more

frequent vortex shedding in the wake. In the case that there are four cylinders in a row (0004-R, 0044-R, 0444-R and 4444-R), the Strouhal number decreases with the increase in the number of rows, since the velocity loss in the cylinder array becomes significant.

3. 4 Model for Description of Overall Features

To describe the interaction process of the shock wave with the cylinder array, the unsteady one-dimensional model[2] is introduced. The governing equations are the one-dimensional Euler equations with the term of the drag force of cylinders and are given in the conservative form:

$$\frac{\partial}{\partial t}\begin{pmatrix}\rho\\ \rho\cdot u\\ E_t\end{pmatrix}+\frac{\partial}{\partial x}\begin{pmatrix}\rho\cdot u\\ \rho\cdot u^2+p\\ (E_t+p)\cdot u\end{pmatrix}=\begin{pmatrix}0\\ -\beta\\ 0\end{pmatrix}, \qquad \cdots\cdots (2)$$

where β represents the drag force of the cylinder array. The gas is assumed to be calorically perfect. The term of the heat flux to the cylinder surface is neglected, since the temperature difference between the flow and the cylinder surface is not large in the present experiments and the effect of the energy exchange between the flow and the cylinders is expected to be negligibly small. In fact, the numerical results considering the heat flux model given in Ref. 2 are almost the same as those without the heat flux term. After Rogg[2], the drag force β is assumed to be in proportion to the local dynamic pressure:

$$\beta=\rho\cdot u^2\cdot B, \qquad \cdots\cdots (3)$$

where B is the drag parameter and represents the drag coefficient per unit length in the flow direction. The drag parameter is assumed to be constant in the cylinder array. This assumption is valid when the cylinders are packed in the channel and the cylinder array is considered as the porous media. The present model is not suitable for coarse cylinder arrangement. The equations (2) and (3) are numerically solved by the finite difference method using Yee's symmetric TVD scheme[7] for the spatial discretization and the two-stage Runge-Kutta method for the time integration. We use the uniform grid with the spacing of 5 mm for computation. The CFL number is set as 0.1.

The drag parameter must be determined by comparison with the experimental data. We consider the cylinder arrangement of the category III (see Table 1). In this category, the porosity ε, which is the volume fraction of void, is considered to be constant at 0.89, since there are four cylinders in each

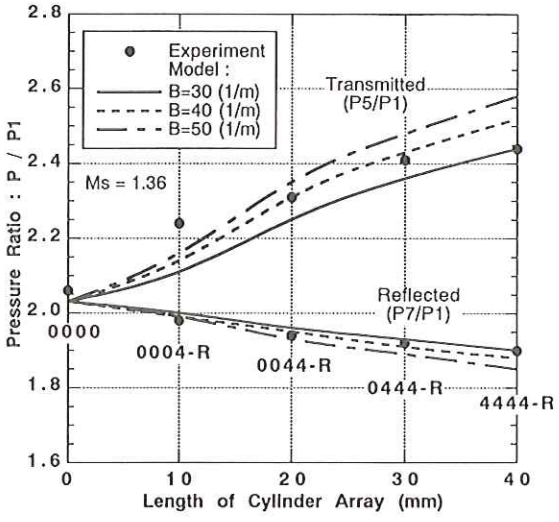

Fig. 25. Comparison of Computational Results with Experimental Data for Pressure behind Transmitted and Reflected Shock Waves

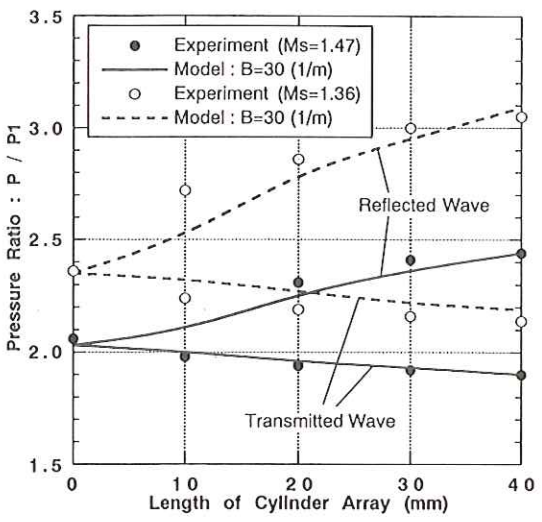

Fig. 26. Comparison of Computational Results with Experimental Data at Shock Mach Numbers 1.36 and 1.47

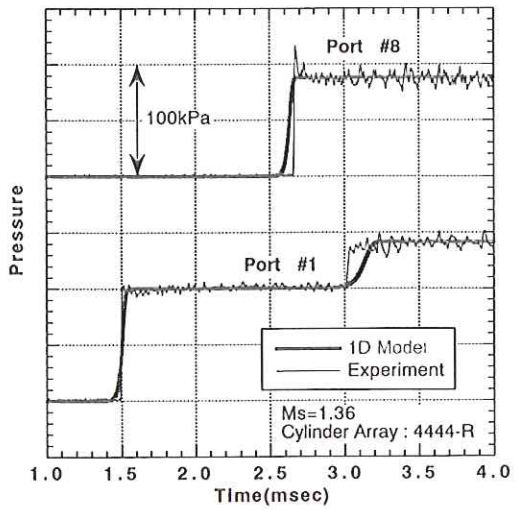

Fig. 27. Comparison of Computational Results with Experimental Data for Pressure Records at Cylinder Arrangement 4444-R

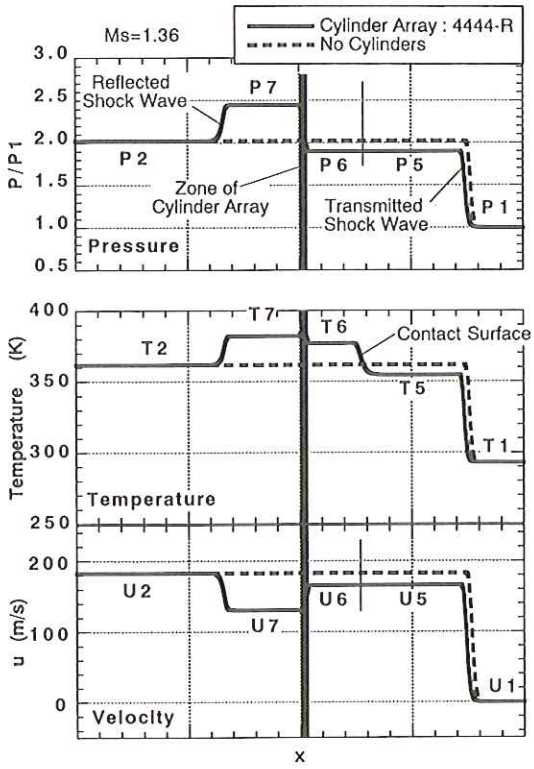

Fig. 28. Spatial Distributions of Pressure, Temperature and Velocity Obtained in Computation

row. The length of the cylinder array is varied from 10 mm (0004-R) to 40 mm (4444-R). The variations of the pressure behind the transmitted shock wave ($P5/P1$) and the pressure behind the reflected shock wave ($P7/P1$) with the length of the cylinder array at the shock Mach number 1.36 are shown in Fig. 25. The results at the shock Mach number 1.47 are shown in Fig. 26. The drag parameter in the range from 30 to 50 m^{-1} provides good agreement with the experimental data both for the transmitted shock wave and for the reflected shock wave. The best fit value of the drag parameter is 30 m^{-1} and 40 m^{-1} for the array length 40 mm and 20-30 mm, respectively.

Figure 27 shows the computational and experimental results on the time history of the pressure at port #1 and #8. The cylinder arrangement is 4444-R. Good agreement is obtained not only on the pressure level but also on the time of arrival of the reflected wave (port #1) and the transmitted wave (port #8). The pressure rise at the shock wave surface is not so sharp in the numerical results due to the insufficient temporal and spatial resolution. It should be noted that the diffusive nature of the reflected shock wave, which is already pointed out in the experimental results in Fig. 9, is also observed in the computational result. The typical spatial distributions of the pressure, temperature and flow velocity are shown in Fig. 28. These patterns are consistent with the wave diagram in Fig. 10. The computational results indicate the presence of the contact surface in the downstream region of the cylinder array. It is expected to correspond to the location of the starting vortices which are observed in the experiments (see Fig. 12).

For the flow resistance of the solid matrix of packed cylinders, some empirical relations[2] are available. These relations are given in terms of the porosity ε, the solid Reynolds number Re_s, and the drag coefficient F defined as follows:

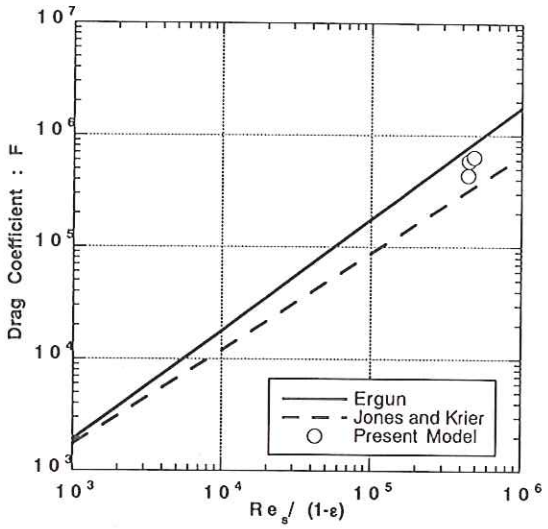

Fig. 29. Variation of Drag Coefficient with Solid Reynolds Number

$$Re_s = \varepsilon \cdot \frac{\rho \cdot u \cdot d}{\mu}, \qquad \cdots\cdots (4)$$

$$F = (B \cdot d) \cdot \frac{Re_s \cdot \varepsilon}{(1-\varepsilon)^2} \cdot \qquad \cdots\cdots (5)$$

Figure 29 shows the comparison of the best fit values of the drag coefficient obtained from Fig. 25 with the relation by Ergun:

$$F = 150 + 1.75 \cdot Re_s/(1-\varepsilon) \qquad (0.4 < \varepsilon < 0.65), \qquad \cdots\cdots (6)$$

and the relation by Jones and Krier:

$$F = 150 + 3.89 \cdot [Re_s/(1-\varepsilon)]^{0.87} \quad (0.38 < \varepsilon < 0.44). \qquad \cdots\cdots (7)$$

Though the porosity in the present experiments is quite large, the present results are close to these relations.

4. CONCLUDING REMARKS

The characteristics of the shock wave propagation through the cylinder array are experimentally investigated by using the shock tube. The unsteady pressure measurement and the flow visualization by the schlieren method are made. The major conclusions are as follows:

(1) In the downstream region of the cylinder array, the attenuation of the transmitted shock wave occurs.

(2) In the upstream region of the cylinder array, the pressure augmentation due to the reflected shock wave occurs. The extent of the pressure augmentation in the upstream region is much stronger than that of the pressure attenuation in the downstream region.

(3) The extent of the pressure attenuation and augmentation mainly depends on the blockage ratio of cylinders in the channel and the length of the cylinder array.

(4) The effects of the staggered arrangement of cylinders are small.

(5) In the wake of the cylinder array, significant pressure oscillation due to the shedding of the Kármán vortices occurs.

(6) The essential features of the propagation process are successfully simulated by the unsteady one-dimensional Euler analysis considering the drag force produced by the cylinder array. The drag

force is evaluated by fitting the numerical results to the experimental data.

ACKNOWLEDGEMENT

The authors would like to express their sincere thanks to Prof. Hinada and Prof. Nakajima of the Institute of Space and Astronautical Science for their suggestion and encouragement to do this study.

REFERENCES

[1] Shimizu, F., Fujii, K. and Higashino, F.: Ground Surface Effect on the Blast Wave Propagation in Two Dimensions, *Trans. Japan Soc. Aero. Space Sci.*, Vol. 36, No. 111, pp. 36-46 (1993).
[2] Rogg, B., Hermann, D. and Adomeit, G.: Shock-Induced Flow in Regular Arrays of Cylinders and Packed Beds, *Int. J. Heat Mass Transfer*, Vol. 28, No. 12, pp. 2285-2298 (1985).
[3] Takayama, K.: Experimental Investigation of Shock Wave / Vortex Interaction at the Shock Wave Research Center, Institute of Fluid Science, Proc. 2nd Int. Workshop on Shock Wave / Vortex Interaction, pp. 244-278 (1998).
[4] Abe, A. and Takayama, K.: Interaction of Shock Waves with Array of Cylinders (in Japanese), Mem. Inst. Fluid Sci., Tohoku Univ., Vol. 10, pp. 109-129 (1999).
[5] Oguchi, H., Funabiki, K. and Sato, S.: An Experiment on the Shock Tube with a Mechanical Shock Valve (in Japanese), Bulletin of Inst. Space and Aeronautical Sci. Univ. Tokyo, Vol. 10, No. 4 (B), pp. 778-786 (1974).
[6] Liepmann, H. W. and Roshko, A.: *Elements of Gas Dynamics*, John Wiley & Sons (1960).
[7] Yee, H. C.: A Class of High-Resolution Explicit and Implicit Shock-Capturing Methods, NASA TM 101088 (1989).